The highly sensitive impedimetric biosensor in label free approach for hepatitis B virus DNA detection based on tellurium doped ZnO nanowires

Fariba Khosravi-Nejad[1] · Maryam Teimouri[2] · Sayeh Jafari Marandi[1] · Mohsen Shariati[3]

Abstract

The highly sensitive impedimetric biosensor in label free approach for hepatitis B virus DNA (HPV DNA) detection based on tellurium doped ZnO nanowires was fabricated. The NWs were grown by hybrid thin film oxidation in the physical vapor deposition (PVD) mechanism. The morphology characterization of the synthesized NWs was performed by field emission scanning electron microscopy (FESEM) and the images demonstrated that the diameter and the length of the materialized NWs were around 50 nm and several micrometers, respectively. The high-resolution transmission electron microscopy (HRTEM) image indicated that the fabricated NWs were crystalline and their phase characterization was validated by the X-ray diffraction pattern (XRD pattern). The single-stranded DNA (ss DNA) probe was immobilized on the surface of the Te-ZnO NWs. The electrochemical impedance spectra (EIS) measurements showed high response sensitivity after hybridization with complementary oligonucleotides. The biosensor could distinguish complementary target from non-complementary and mismatch oligonucleotides. The HBV biosensor could respond to complementary target in the concentrations range from 1 pM to 1 μM. The limit of detection (LOD) of the biosensor was 0.1 pM. The stability of the HBV DNA biosensor was investigated and biosensor could show 95% of its initial responses after 8 weeks maintenance.

1 Introduction

Hepatitis B virus (HBV) as a DNA virus is a type of the genus Orthohepadnavirus and a portion of the Hepadnaviridae type of viruses, [1]. The hepatitis B disease is originated from the HBV. The viral hepatitis caused by HBV is identified as a serious public health challenge in the world and has caused some dangerous results counting cirrhosis and hepatocellular carcinoma, [1]. Currently, around half of one billion people have been infected by the HBV and this virus affects the mortality generated by liver disease which has infected around one million people annually, [1]. Recently, the intensive attentions and respects have been centralized on the HBV detection and materialization of the diagnosis systems, [1]. The nano-based materials and technologies have acquired significant attentions in resolving the challenges related to the DNA detection, especially HBV diagnosis, [1].

Zinc oxide as a semiconductor metal oxide, with $E_{g\sim}3.37$ eV, is one of the most significant semiconductors, [2]. Due to the outstanding performances of the zinc oxide in the optoelectronics and biotechnology, ZnO NWs have been potential candidates for wide applications and performances such as UV lasers, the electrochemical and transistor-based gas sensors and biosensors, [3]. Recently, ZnO NWs have shown the impressive physicochemical current and photoelectrical applications, [3–7]. The electronic, magnetic and optical properties of ZnO NWs could be altered effectively by doping with various transition metals injection. The previous reports have indicated that tellurium metal co-doping with zinc metal could enhance the emission caused by acceptor and donor, [8]. The acceptor and donor are the non-radiative recombination in ZnO nano and microstructures in which the electrical properties of the ZnO could increase the electrochemical performances of the bio-sensing and detection, [1, 8]. The defects are the main vacancy parameters

✉ Fariba Khosravi-Nejad
  fkhosravinejad@riau.ac.ir

1 Department of Biology, Faculty of Biosciences, North Tehran Branch, Islamic Azad University, Tehran, Iran

2 Department of Biology, Roudehen Branch, Islamic Azad University, Roudehen, Iran

3 Institute for Nanoscience and Nanotechnology, Sharif University of Technology, 14588-89694 Tehran, Iran

which are comparatively passivated by the iso-electronic doping of the tellurium, [9]. The photo-catalytic operational performances of the undoped and doped ZnO were investigated by the degradation of brilliant green (BG). The past works of the degradation showed that the Te-ZnO hybrid structure has high photo-catalytic performance in comparison to undoped ZnO, [10–12].

Recently, ZnO nanostructures (NSs) in flower-like shape were investigated to the detection of the bacterial meningitis by electrochemical measurement system, [13]. A biosensor based on ZnO-carbon nanotubes nanocomposite was used to the meningitis DNA detection via EIS measurements, [14]. The hybrid structure based on nickel-ZnO film was investigated to biosensor fabrication for the meningitis DNA diagnosis, [15]. A DNA biosensor was materialized using APTES with ZnO NSs fabricated via chemical vapor deposition (CVD) growth mechanism for electrochemical biosensor approach and purpose, [16].

In this paper, the biosensor properties of Te-ZnO NWs for HBV DNA detection in EIS diagnosis measurement system is investigated. The NWs were fabricated via PVD growth technique in the tubular furnace under controlled situations [17]. The stable and reproducible Te-ZnO NWs-based biosensor with intensive sensitivity is introduced. The probe DNA was immobilized on the surface of the NWs and the hybridization process with DNA complementary target was analyzed. The EIS measurements demonstrated high sensitivity after hybridization with DNA target. The biosensor could discern among complementary, non-complementary and mismatch HBV DNA sequences targets. The biosensor responded to complementary DNA sequences in the very low concentrations. The biosensor showed interesting reproducibility.

2 Experimental

### 2.1 The fabrication of Te-doped ZnO NWs

For Te-doped ZnO NWs fabrication in this research, the granule zinc and tellurium metals were used. The controllable technique for NWs growth was sputtering deposition technique associated with annealing process in tubular furnace under controlled vacuum. The nucleation sites for aligned NWs growth were created in annealing mechanism. The applied technique for Te-doped ZnO NWs fabrication prepares the nucleation sites for preferred growth direction and desired alignment.

The silicon substrates (Si substrates), p-type, were used to NWs growth. They were washed and cleansed in ethanol and de-ionized water and sonicated in ultrasonic bath for 25 min. The sputtering system with radio frequency generator (RF sputtering) was operated in 13.56 MHz frequency. The zinc

and tellurium metals with 99.999% purity were used. The schematic image of RF sputtering is shown in Fig. 1a. To film fabrication; a three-step technique was applied. First zinc metal was sputtered. Second tellurium metal was filmed and then zinc metal was sputtered again. The pre-conditions of the experiment were chamber pressure in 6×10^{-6} mbar and temperature at 135 °C. After the 35 Sccm argon gas introduction, the chamber working pressure and temperature were reached to 5×10^{-2} mbar and 163 °C, respectively. The system was maintained at 110 °C temperature. The three-layer thin film was 5 μm in thickness (90% Zn and 10% Te).

The annealing step was performed after the RF-sputtering deposition process. The fabricated thin film was annealed in the horizontal furnace, Fig. 1b. The annealing process was materialized under oxygen flow and high temperature. The synthesized Zn-Te film was heat treated in the horizontal furnace at 1400 °C in Ar:O_2 presence (10:1 ratio) for 85 min.

For characterization of the grown Te-doped ZnO NWs, a FESEM microscope (TESCAN model: MIRA2) was used. The phase structure of the NWs was analyzed by An X-ray
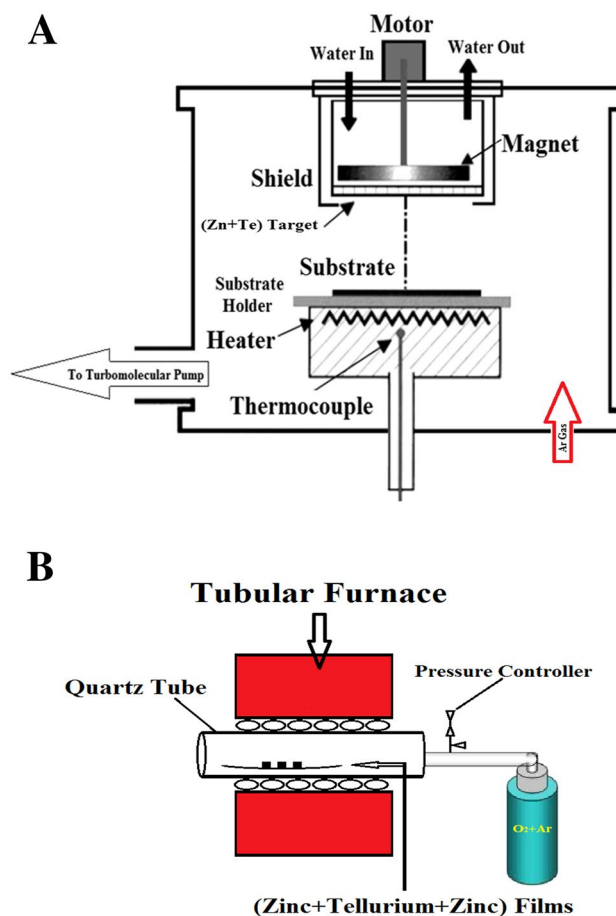
Fig. 1 **a** The schematic picture of the RF magnetron sputtering, **b** the horizontal furnace for annealing process in O_2 + Ar presence, and the NWs materialization process

diffractometer (Rigaku D/max RB). A TEM microscope (Philips, CM-30) was applied to realize the crystallographic growth directions and morphological parameters of the Te-doped ZnO NWs. The electrochemical impedance measurements were performed using a potentiostat (PG STAT302N, module FRA32M; frequency response analyzer) with a conventional three-electrode test cell. The Ag/AgCl electrode was used as a reference electrode, the platinum electrode was utilized as counter electrode and the Te-doped ZnO NWs as working electrode. The EIS electrolyte was 0.2 M KCl buffered solution containing 2 mM $K_4Fe(CN)_6/K_3Fe(CN)_6$ (1:1). The EIS measurements were performed in open circuit potential over the frequency range 0.01–100 kHz with the modulation of $+10$ mV. The EIS bio-sensing experiments were investigated 3 times at room temperature.

2.2 2. Oligonucleotides immobilization and hybridization process on the NWs surface

To immobilize the DNA probe on the surface of the Te-doped ZnO NWs, first ssDNA oligonucleotides were positioned in dithiothreitol (D.T.T) solution diluted in phosphate-buffered saline (PBS) with pH ~ 8.4 in 0.1 M volume for 30 min. The D.T.T solution was used to segregate the disulfide bonds of the thiolated DNA probe. The 1 µL volume of the ssDNA (1 µM) in Tris–EDTA (T.E) buffer was immobilized on the Te-doped ZnO NWs electrode surface. The T.E buffer was 10 mM Tris–HCl, 1 mM EDTA in pH ~ 8.2. In order to inhibit Te-doped ZnO NWs surface from contaminating, the NWs electrode was maintained in the sealed box. The electrodes were maintained in 8 h under controlled environment and cleansed with DIW at room temperature. For the probe hybridization with different DNA oligonucleotides targets, the 1 µL volume of the targets (concentrations range from 1 pM to 1 µM) in saline-sodium citrate (SSC) buffer (pH ~ 7.1) was pasted on the probe-modified NWs electrode surface, and the electrode was kept in the sealed box. Finally, the biosensor Te-doped ZnO NWs electrode was cleansed by SSC and the electrochemical measurements were conducted. The used DNA sequences (probe and different targets) are listed in Table 1. The sequence of oligonucleotides was selected using basic local alignment search tool (BLAST) to have the least similarity to the human serum genome. To select these types of

the DNA oligonucleotides, their spatial symmetry and thermodynamical aspects, which prevents them from screwing or bending when immobilized to the surface, were significant parameters, [18].

3 Results and discussion

3.1 1. Morphology, structure and phase characterization

The morphology characterization of the Te-doped ZnO NWs is depicted in Fig. 2. The Te-doped ZnO NWs were synthesized on the Si substrate. The fabricated Te-doped ZnO NWs are 50 nm in diameter and several micrometers in the length, Fig. 2. The density of the Te-doped ZnO NWs on the surface is very high. The grown NWs are in satisfying wire shape. They are uniformly distributed on the surface of the silicon substrate.

Figure 3 indicates the crystallographic analysis and structural measurement of the Te-doped ZnO NWs using a TEM microscope. The TEM image of Te-doped ZnO NWs from selected sample with a diameter size of around 50 nm and the corresponding HRTEM image of the NWs are shown in Fig. 3. The HRTEM image indicates that the NWs are highly crystalline, and the tellurium dopant did not result any significant crystallographic defects or other mismatches. The HRTEM image confirms the wurtzite structure of the Te-doped ZnO NWs. The crystallinity of the fabricated NWs was also validated by spotting the lattice spacing of 0.263 nm in HRTEM image shown in Fig. 3 inset. This measurement is in comparison to the 0.26 ± 0.05 nm lattice spacing for ZnO corresponding to (101) which is the standard growth plane of wurtzite zinc oxide.

To validating the crystallographic phase, the selected area electron diffraction (SAED) analysis was performed. The SAED measurement was applied to investigate the crystallographic structure of the Te-doped ZnO NWs by identifying the zone axis of SAED pattern. The inset image in the Fig. 3 is the SAED pattern corresponding to the zone axis which was [001]. The SAED pattern was coincided with HHRTEM measurement.

Figure 4 demonstrates the XRD pattern measurements of the Te-doped ZnO NWs. The XRD pattern in Fig. 4

Table 1 DNA oligonucleotides

Sequence name	Sequence of oligonucleotides	Company (Country)
Probe (thiolated)	5′—HS $(CH_2)_6$ TAC CGT CCC CTT CTT CAT CTG CCG T- 3′	Bioneer (Republic of Korea)
Complementary target	5′—ACG GCA GAT GAA GAA GGG GAC GGT A - 3′	Bioneer (Republic of Korea)
Mismatch target (One-Point)	5′—ACG CCA GAT GAA GAA GGG GAC GGT A - 3′	Bioneer (Republic of Korea)
Non-complementary Target	5′—TAC CGT CCC CTT CTT CAT CTG CCG T - 3′	Bioneer (Republic of Korea)

Fig. 2 The FESEM images of Te-doped ZnO NWs sample. **a** The FESEM image of the Te-doped ZnO NWs in the end of annealing process. **b** The diameter size of the NWs is around 50 nm and several microns in length
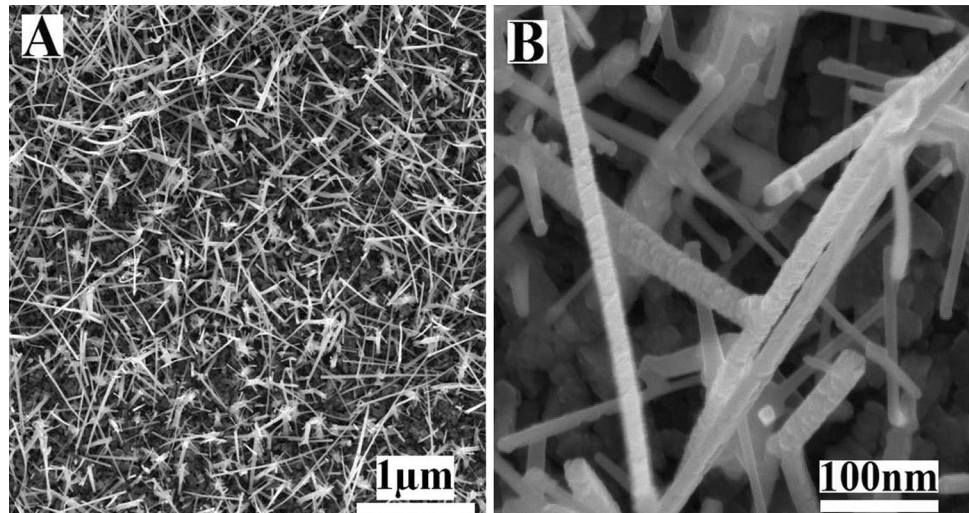
Fig. 3 **a** The TEM image of Te doped ZnO NWs. **b** The high resolution TEM image of signed part on the NWs. The inset; the corresponding SAED pattern (zone axis of SAED pattern was [001])
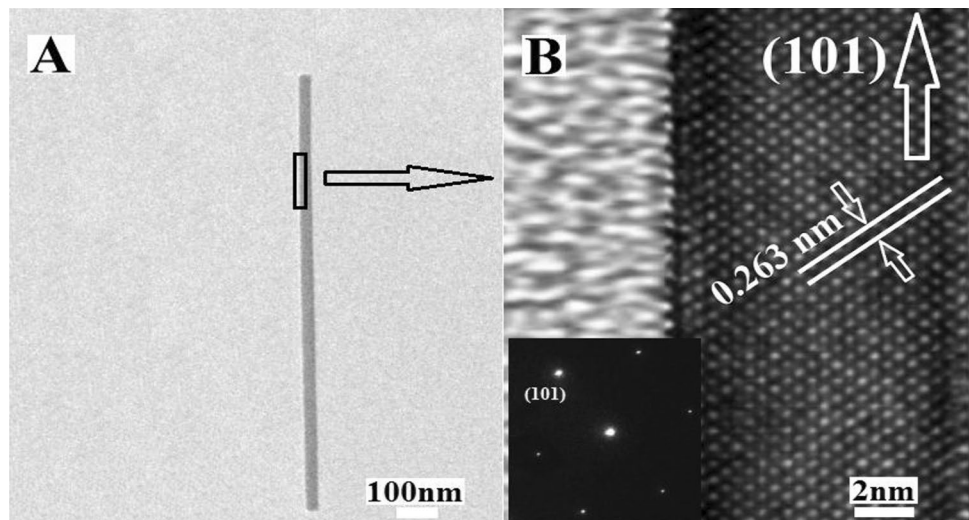

corresponds with the standard parameters of the bulk wurtzite zinc oxide. This pattern validated two involved material phases: one of them corresponding to the hexagonal wurtzite phase of ZnO (lattice constants $a = 3.24982$ Å, $c = 1.6021$ Å, JCPDS No. 361,451)) and the other corresponding to the rutile structure of TeO_2 (JCPDS No. 78–1713). All indexed peaks in the XRD pattern were contributed to the wurtzite phase of ZnO–TeO_2 hetero-structure. Therefore, the XRD results revealed that the fabricated outcome could be hetero-structure ZnO–TeO_2 NWs. The intensity of the peaks in XRD pattern for the zinc oxide spectrum is higher than tellurium oxide.

The most significant peak at $2\theta = 36.40°$ is indexed to (101) crystallographic plane in zinc oxide wurtzite phase structure.

3.2 The Electrochemical DNA biosensor characterization

3.2.1 The EIS selectivity studies of the Te-doped ZnO NWs electrode

The selectivity of the materialized DNA Te-doped ZnO NWs biosensor was investigated. For measuring the selectivity of the fabricated biosensor with DNA sequences, the
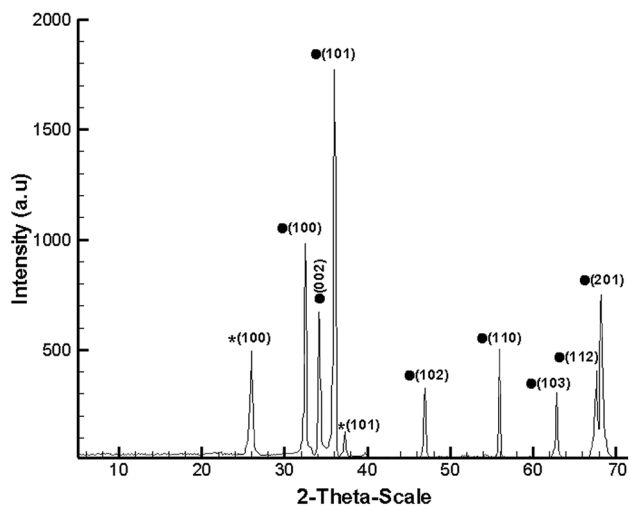
Fig. 4 The XRD pattern of the Te-doped ZnO NWs. All indexed peaks in the XRD spectrum contribute to the wurtzite phase of ZnO–TeO$_2$ heterostructure. The star sign related to TeO$_2$ and solid circle to ZnO

hybridization of the mismatched, non-complementary and complementary DNA oligonucleotides targets with the probe were investigated. The selectivity as a critical factor of the biosensor was measured under controlled situations. Figure 5 shows the EIS spectra (Nyquist mode by redox maker ions) for the Te-doped ZnO NWs electrode modified with probe. The inset in the Fig. 5 demonstrates

the Randle's equivalent circuit. In the Randle's circuit, R_{ct} is the charge transfer resistance as semi-circle diameter of the Nyquist plot, C_{DL} is the double layer capacitor in the interface between electrode and solution and R_S is the solution resistance. The warburg impedance (Z_W) originates from the redox couple diffusion and the electrode at low frequencies, [19]. All the selectivity bio-sensing tests were performed in 1 μM concentration.

The R_{ct} was enhanced by the hybridization of the probe sequences on the surface of the Te-doped ZnO NWs electrode with ds-DNA, Fig. 5. In Te-doped ZnO NWs electrode the corresponding R_{ct} was decreased from 5016 to 4267 Ω for complementary and mismatch targets after hybridization with the probe. The electrostatic interactions between the redox maker ions and the Te-doped ZnO NWs (repulsive interactions) were the main factors which significantly influenced the R_{ct} alterations. The charge transfer in complementary hybridization had been hindered by repulsion through the interface, [19]. The ssDNA- Te-doped ZnO NWs hybrid electrode showed the lowest R_{ct}. The R_{ct} of the functionalized probe surface was 1583 Ω. The main factors involved in R_{ct} alternations are the electrostatic and steric repulsion. These factors caused the charge transfer enhancement between electrolyte and the electrode. Therefore, the electrostatic and steric repulsion are reasons which probe modified electrode showed intensive charge transfer. This intensive charge transfer reduced the semicircle diameter of the EIS spectrum diagram, [2–4]. Due to weak complementary

Fig. 5 The EIS impedance spectra of DNA oligonucleotides. The mismatch, non-complementary and complementary target DNA oligonucleotides hybridization measured for Te-doped ZnO NWs electrode with 1 μM concentration
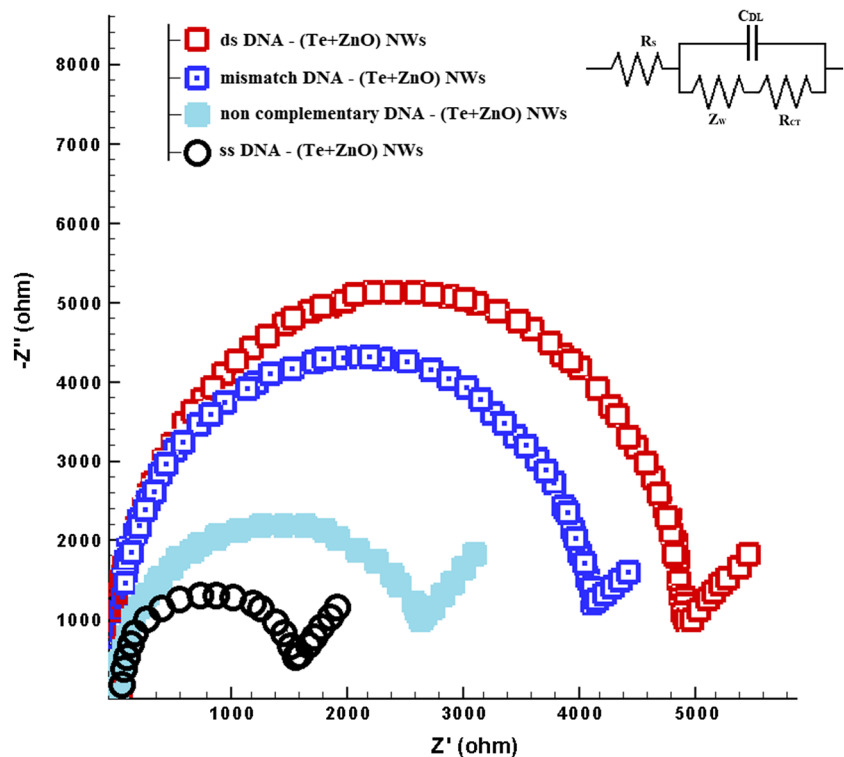
duplex materialization between non-complementary DNA oligonucleotides and Te-doped ZnO NWs surface, the weak hybridization has been demonstrated in comparison to complementary and mismatched oligonucleotides and the R_{ct} value was around 2739 Ω.

3.2.2 The EIS sensitivity of the Te-doped ZnO NWs electrode

The sensitivity of the Te-doped ZnO NWs electrode was investigated. The measurements were investigated by testing the response sensitivity of biosensor to various concentrations of complementary target oligonucleotides. The sensitivity of biosensor to the complementary sequences was measured for the Te-doped ZnO NWs, from 1 pM to 1 μM, Fig. 6. The Te-doped ZnO NWs electrode could detect lowest concentration of the 1 pM. The R_{ct} values were enhanced with the augmentation of the complementary DNA target concentration. The Te-doped ZnO NWs biosensor showed high sensitivity in concentrations over the range from 1 pM to 1 μM, Fig. 6.

3.2.3 Reproducibility and stability studies of the Te-doped ZnO NWs electrode

By calculating the materialized data from three independent electrodes fixed in 1 nM concentration, the reproducibility of the Te-doped ZnO NWs electrode biosensor in DNA sensing

were investigated. The relative standard deviation (RSD) values for Te-doped ZnO NWs were 1.03% and 3.63% and 4.85% for non-complementary, mismatch and complementary targets, respectively. The RSD values lower than 9% showed that the Te-doped ZnO NWs electrode has excellent reproducibility in bio-sensing diagnosis in comparison to previous reports, [2].

Figure 7 indicates the calibration curve (ΔR_{ct} vs. the log scale of the concentration). The linear relation between the ΔR_{ct} and the log scale of complementary DNA sequences concentrations in Te-doped ZnO NWs electrode was investigated (black line). The stability of the HBV DNA biosensor was investigated by storing the biosensor in the freezer at 4 °C and biosensor could show 95% of its initial responses after 8 weeks maintenance (red line). This showed that the Te-doped ZnO NWs biosensor responses had longstanding stability. Figure 7 illustrates that the variations of ΔR_{ct} values have a linear relation with the logarithm of target HBV concentrations over the range from 1 pM to 1 μM. The 0.1 pM LOD can be estimated for the Te-doped ZnO NWs. They were estimated via adding S_b and $3\sigma_b$; where S_b is the signal of blank and σ_b is the standard deviation of blank.
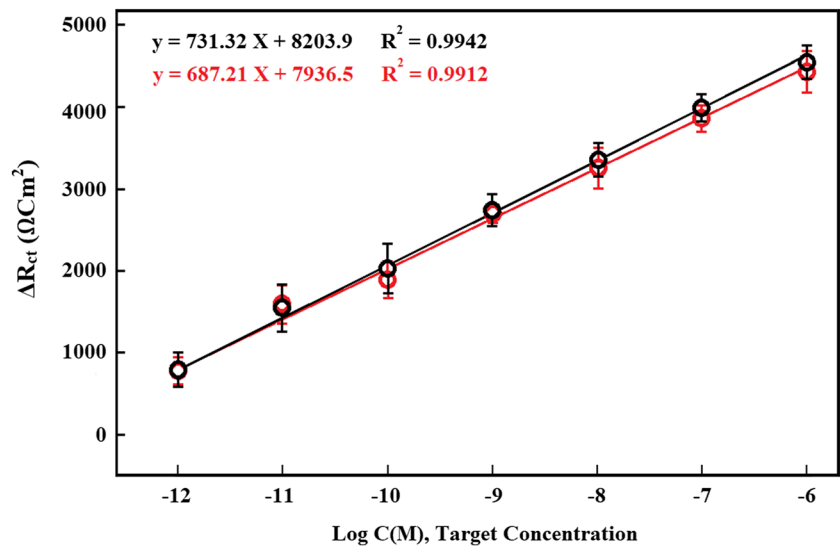
Table 2 shows the summary of the Randle's equivalent circuit parameters for the Te-doped ZnO NWs electrode.

Table 3 shows the comparison between some DNA biosensors for labeled and label-free detection mechanisms. As seen in Table 3, the present biosensor has a low LOD and wide linear range, comparable to other biosensors. The high

Fig. 6 The EIS measurements of the Te-doped ZnO NWs electrode; the sensitivity of biosensor to the complementary oligonucleotides measured for Te-doped ZnO NWs, from 1 pM to 1 μM
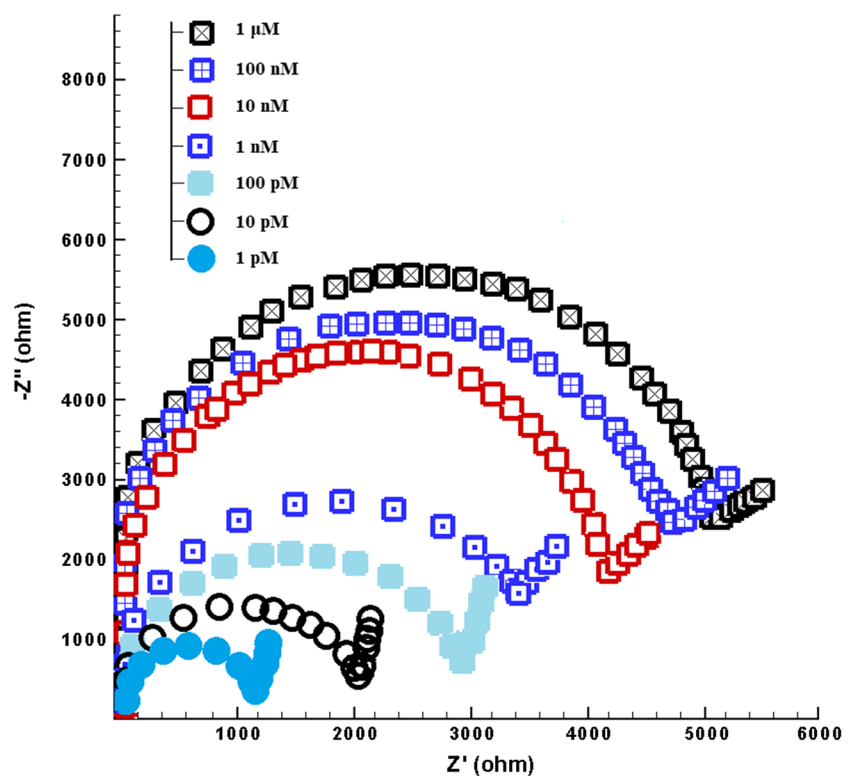
Fig. 7 The linear relation between the ΔR_{ct} and the log scale of complementary DNA sequences concentrations in Te-doped ZnO NWs electrode (black line). The stability of the Te-doped ZnO NWs biosensor after 8 weeks maintenance (red line)

y = 731.32 X + 8203.9 R^2 = 0.9942
y = 687.21 X + 7936.5 R^2 = 0.9912

Table 2 The summary of the Randle's equivalent circuit parameters for the Te-doped ZnO NWs electrode

Sample	$R_S (\Omega)$	C_{DL} (μF)	N	$R_{ct} (\Omega)$	RSD value	Z_W
SS-DNA	181	0. 297	0.79	1583	0.36%	0.0518
DS-DNA	562	0. 126	0.73	5016	4.21%	0.0246

Table 3 The Comparison of the different biosensors for DNA detection

Biosensor	Limit of detection (LOD)	Linear range	Technique description	References
DNA biosensor based on silicon nanowires	10 pM	10 pM –100 nM	Solution-gated field-effect transistor	[20]
PNA-DNA biosensor based on silicon nanowires	10 fM	10 fM–1 μM	Concentration-dependent resistance	[21]
MiRNAs biosensor based on silicon nanowires	1 fM	1fM–1 nM	Nanowire-based field-effect sensors	[22]
Nucleic acids biosensor based on silicon nanowires	0.1 fM	0.1 fM–100 nM	SiNW-FETs field effect transistor biosensors	[23]
15-base single-strand DNA Molecules biosensor based on silicon nanowire	0.1 fM	0.1 fM–2 pM	Nanowire-based field-effect sensors	[24]
Nucleic Acids Nanobiosensor based on silicon nanowire	1 fM of target DNA	1 fM–1 nM	SiNWs Field-Effect Transistor Nanosensors	[25]
DNA biosensor based on Carbon Nanotube	1 pM	1–10 pM	Carbon nanotubes FET	[26]
DNA influenza A virus DNA biosensor based on Carbon Nanotube	1 pM	1 pM–10 nM	CNT field effect transistor based DNA sensor	[27]
DNA biosensor based on graphene/Si-nanowires diode-type	0.1 pM	0.1–500 nM	Graphene/surface modified vertical-Si-NW-arrays junctions as diode-type biosensors	[28]
Hepatitis B virus DNA biosensor based on tellurium doped ZnO nanowires	0.1 pM	1 pM to 1 μM	Electrochemical impedance spectra based on tellurium doped ZnO nanowires	This work

surface ratio for Te-doped ZnO NWs was the main factor in the high sensitivity of the HBV DNA biosensor.

4 Conclusion

In this paper, the highly sensitive HBV DNA impedimetric biosensor based on Te-doped ZnO was reported.

The biosensor properties of Te-doped ZnO NWs for HBV detection via EIS measurements were investigated. The FESEM and HRTEM images associated with XRD pattern indicated that the fabricated NWs were crystalline. The fabricated biosensor showed good stability and high reproducibility in very low concentration. The LOD of the HBV biosensor was 0.1 pM. The biosensor could distinguish among complementary target, non-complementary and mismatch HBV DNA oligonucleotides.

5. References

1. M. Shariati, The field effect transistor DNA biosensor based on ITO nanowires in label-free hepatitis B virus detecting compatible with CMOS technology. Biosens. Bioelectron. **105**, 58–64 (2018)
2. F. Lu, W. Cai, Y. Zhang, ZnO, hierarchical micro/nanoarchitectures: solvothermal synthesis and structurally enhanced photocatalytic performance. Adv. Funct. Mater. **18**, 1047 (2008)
3. Y. Zhang, M.K. Ram, E.K. Stefanakos, D.Y. Goswami, Synthesis, characterization, and applications of ZnO nanowires. J. Nanomater. **2012**, 624520 (2012)
4. M. Azarang, A. Shuhaimi, R. Yousefi, M. Sookhakian, Effects of graphene oxide concentration on optical properties of ZnO/RGO nanocomposites and their application to photocurrent generation. J. Appl. Phys. **116**, 084307 (2014)
5. M. Furuta, Y. Kamada, M. Kimura, S-i Shimakawa, T Kawaharamura, D Wang, C Li, S Fujita, T Hirao, Photocurrent and persistent photoconductivity in zinc oxide thin-film transistors under ultraviolet-light irradiation. Jpn. J. Appl. Phys. **50**, 110204 (2011)
6. J. Katayama, M. Izaki, Observation of photocurrent generation in electrodeposited zinc oxide layers. J. Appl. Electrochem. **30**, 855–858 (2000)
7. K. Keem, H. Kim, G.-T. Kim, J.S. Lee, B. Min, K. Cho, M.-Y. Sung, S. Kim, Photocurrent in ZnO nanowires grown from Au electrodes. Appl. Phys. Lett. **84**, 4376 (2004)
8. S.-H. Park, T. Minegish, D.-C. Oh, J.-H. Chang, T. Yao, T. Taishi, I. Yonenaga, p-type conductivity control of heteroepitaxially grown ZnO films by N and Te codoping and thermal annealing. J. Cryst. Growth **363**, 190–194 (2013)
9. A. Iribarren, P. Fernández, J. Piqueras, Recombination processes in Te-doped ZnO microstructures. Phys. Status Solidi B **251**, 683–688 (2014)
10. A. Iribarren, P. Fernandez, J. Piqueras, Cathodoluminescence study of Te-doped ZnO microstructures grown by a vapour–solid process. J. Mater. Sci. **43**, 2844–2848 (2008)
11. F. Jamali-Sheini, R. Yousefi, M.R. Mahmoudian, N.A. Bakr, A. Saaedi, N.M. Huang, Facile synthesis of different morphologies of Te-doped ZnO nanostructures. Ceram. Int. **40**, 7737–7743 (2014)
12. N. Shanmugam, S. Suthakaran, N. Kannadasan, K Sathish Kumar, synthesis and characterization of Te doped ZnO nanosheets for photocatalytic application. J. Heterocycl. **1**(1), 1–6 (2015)
13. M. Tak, V. Gupta, M. Tomar, Flower-like ZnO nanostructure based electrochemical DNA biosensor for bacterial meningitis detection. Biosens. Bioelectron. **59C**, 200–207 (2014)
14. M. Tak, V. Gupta, M. Tomar, A ZnO–CNT nanocomposite based electrochemical DNA biosensor for meningitis detection. RSC Adv. **6**, 76214–76222 (2016)
15. M. Tak, V. Gupta, M. Tomar, An electrochemical DNA biosensor based on Ni doped ZnO thin film for meningitis detection. J. Electroanal. Chem. **792**, 8–14 (2017)
16. A.M. Mohammed, I.J. Ibraheem, A.S. Obaid, M. Bououdina, Nanostructured ZnO-based biosensor: DNA immobilization and hybridization. Sens. Bio Sens. Res. **15**, 46–52 (2017)
17. F. Khosravi-Nejad, M. Teimouri, S.J. Marandi, M. Shariati, The highly crystalline tellurium doped ZnO nanowires photodetector. J. Cryst. Growth **522**, 214–220 (2019)
18. Z. Shakoori, S. Salimian, S. Kharrazi, M. Adabi, R. Saber, Electrochemical DNA biosensor based on gold nanorods for detecting hepatitis B virus. Anal. Bioanal. Chem. **407**(2), 455–461 (2015)
19. Z.G. Gokce, P. Akalın, F.N. Kok, A.S. Sarac, Impedimetric DNA biosensor based onpolyurethane/poly(m-anthranilic acid) nanofibers. Sens. Actuat. B **254**, 719–726 (2018)
20. Y.L. Bunimovich, Y.S. Shin, W.S. Yeo, M. Amori, G. Kwong, J.R. Heath, Quantitative real-time measurements of DNA hybridization with alkylated nonoxidized silicon nanowires in electrolyte solution. J. Am. Chem. Soc. **128**, 16323–16331 (2006)
21. G.J. Zhang, J.H. Chua, R.E. Chee, A. Agarwal, S.M. Wong, K.D. Buddharaju, N. Balasubramanian, Highly sensitive measurements of PNA-DNA hybridization using oxide-etched silicon nanowire biosensors. Biosens. Bioelectron. **23**, 1701–1707 (2008)
22. G.J. Zhang, J.H. Chua, R.E. Chee, A. Agarwal, S.M. Wong, Label-free direct detection of MiRNAs with silicon nanowire biosensors. Biosens. Bioelectron. **24**, 2504–2508 (2009)
23. A. Gao, N. Lu, Y. Wang, P. Dai, T. Li, X. Gao, Y. Wang, C Fan Enhanced sensing of nucleic acids with silicon nanowire field effect transistor biosensors. Nano Lett. **12**, 5262–5268 (2012)
24. C.J. Chu, C.S. Yeh, C.K. Liao, L.C. Tsai, C.M. Huang, H.Y. Lin, J.J. Shyue, Y.T. Chen, CD Chen Improving nanowire sensing capability by electrical field alignment of surface probing molecules. Nano Lett. **13**, 2564–2569 (2013)
25. A. Gao, N. Lu, P. Dai, T. Li, H. Pei, G.G. Xiuli, W.Y. Yuelin, F. Chunhai, Silicon-nanowire-based CMOS-compatible field-effect transistor nanosensors for ultrasensitive electrical detection of nucleic acids. Nano Lett. **11**, 3974–3978 (2011)
26. C.T. Xuan, N.T. Thuy, T.T. Luyen, T.T. Huyen, M.A. Tuan, Carbon nanotube field-effect transistor for DNA sensing. J. Electron. Mater. **46**, 3507–3511 (2017)
27. T.L. Tran, T.T. Nguyen, T.H. Tran, V.T. Chu, Q.T. Tran, A.T. Mai, Detection of influenza a virus using carbon nanotubes field effect transistor based DNA sensor. Phys. E **93**, 83–86 (2017)
28. J. Kim, S.-Y. Park, S. Kim, D.H. Lee, J.H. Kim, J.M. Kim, K H, Han J-S, Park JW, Lee H, Choi S-H, Precise and selective sensing of DNA-DNA hybridization by graphene/Si-nanowires diode-type biosensors. Sci. Rep. **6**, 31984 (2016)